The Astrophysical Journal, 798:80 (12pp), 2015 January 10 doi:10.1088/0004-637X/798/2/80

FORMATION OF S-BEARING SPECIES BY VUV/EUV IRRADIATION OF H_2S-CONTAINING ICE MIXTURES: PHOTON ENERGY AND CARBON SOURCE EFFECTS

Y.-J. Chen[1,2,*], K.-J. Juang[1], M. Nuevo[3,4], A. Jiménez-Escobar[5], G. M. Muñoz Caro[5], J.-M. Qiu[1], C.-C. Chu[1], T.-S. Yih[1], C.-Y. R. Wu[2], H.-S. Fung[6], and W.-H. Ip[7]

[1] Department of Physics, National Central University, Jhongli City, Taoyuan County 32054, Taiwan
[2] Space Sciences Center and Department of Physics and Astronomy, University of Southern California, Los Angeles, CA 90089-1341, USA
[3] NASA Ames Research Center, Moffett Field, CA 94035, USA
[4] BAER Institute, Petaluma, CA 94952, USA
[5] Centro de Astrobiología, INTA-CSIC, Torrejón de Ardoz, E-28850 Madrid, Spain
[6] National Synchrotron Radiation Research Center, Hsinchu 30076, Taiwan
[7] Graduate Institute of Astronomy, National Central University, Jhongli City, Taoyuan County 32049, Taiwan
Received 2013 December 26; accepted 2014 October 27; published 2014 December 24

ABSTRACT

Carbonyl sulfide (OCS) is a key molecule in astrobiology that acts as a catalyst in peptide synthesis by coupling amino acids. Experimental studies suggest that hydrogen sulfide (H_2S), a precursor of OCS, could be present in astrophysical environments. In the present study, we used a microwave-discharge hydrogen-flow lamp, simulating the interstellar UV field, and a monochromatic synchrotron light beam to irradiate CO:H_2S and CO_2:H_2S ice mixtures at 14 K with vacuum ultraviolet (VUV) or extreme ultraviolet (EUV) photons in order to study the effect of the photon energy and carbon source on the formation mechanisms and production yields of S-containing products (CS_2, OCS, SO_2, etc.). Results show that (1) the photo-induced OCS production efficiency in CO:H_2S ice mixtures is higher than that of CO_2:H_2S ice mixtures; (2) a lower concentration of H_2S enhances the production efficiency of OCS in both ice mixtures; and (3) the formation pathways of CS_2 differ significantly upon VUV and EUV irradiations. Furthermore, CS_2 was produced only after VUV photoprocessing of CO:H_2S ices, while the VUV-induced production of SO_2 occurred only in CO_2:H_2S ice mixtures. More generally, the production yields of OCS, H_2S_2, and CS_2 were studied as a function of the irradiation photon energy. Heavy S-bearing compounds were also observed using mass spectrometry during the warm-up of VUV/EUV-irradiated CO:H_2S ice mixtures. The presence of S-polymers in dust grains may account for the missing sulfur in dense clouds and circumstellar environments.

Key words: astrochemistry – methods: laboratory: molecular – molecular processes – ultraviolet: ISM

1. INTRODUCTION

Theoretical gas-phase chemistry models require very low sulfur abundances in order to match the observations of S-bearing gas-phase molecules in dense molecular clouds (Millar & Herbst 1990). Garozzo et al. (2010) suggested that the missing sulfur is probably locked in icy grain mantles, and later rapidly destroyed to form SO_2 and OCS and other sulfur-bearing molecules by cosmic-ray irradiation. However, there are no observations that support this suggestion; so far, only OCS and tentatively SO_2 have been detected in icy grain mantles (Palumbo et al. 1995, 1997; Boogert et al. 1996, 1997; Zasowski et al. 2009). On the other hand, several S-bearing molecules such as NS, SO, SO_2, H_2S, H_2CS, OCS, and HCS^+ were observed in the gas phase of hot cores (van der Tak et al. 2003), but current gas-phase chemical models are unable to explain the abundances of some S-bearing molecules like OCS and HCS^+ observed toward protostars (Doty et al. 2004). One hypothesis is that S-bearing molecules are formed in ice mantles and later released to the gas phase (Grim & Greenberg 1987; Jiménez-Escobar et al. 2011). Laboratory experiments show that S-polymers S_6 through S_8 are present in residues produced from the UV irradiation of H_2O:CO:NH_3:H_2S ices and subsequent warm-up, together with S_5CH_2, S_6CH_2, and c-(S–CH_2–NH–CH_2–NH–CH_2), which are all detected using gas chromatography (Muñoz Caro 2002). More recently, Jiménez-Escobar et al. (2011) reported the formation of S_2 and S_3 in UV-irradiated H_2S and H_2O:H_2S ices, which were observed during subsequent warm-up process. The sulfur dimer, S_2, has also been detected in X-ray-irradiated H_2S ices (Jiménez-Escobar et al. 2012).

The formation of OCS, which was detected in ice mantles due to its unusually high IR band strength, has been studied by the proton irradiation of CO:H_2S, CO_2:H_2S, CO:SO_2, and CO_2:SO_2 ice mixtures (Ferrante et al. 2008; Garozzo et al. 2010). Those experiments show that the production of OCS is more efficient in H_2S-containing ice mixtures than in SO_2-containing ice mixtures. The main purpose of the present study is to identify which ice component and photon energy lead to the production of the highest abundance of OCS. Interestingly, Leman et al. (2004) reported that OCS can catalyze the coupling of amino acids toward the production of peptides. Amino acids are known to form from the vacuum ultraviolet (VUV) and/or extreme ultraviolet (EUV) irradiation of ice mixtures containing H_2O, NH_3, and one or more carbon sources among CO, CO_2, CH_3OH, CH_4, and even naphthalene ($C_{10}H_8$) (Bernstein et al. 2002; Muñoz Caro et al. 2002; Nuevo et al. 2007, 2008; Chen et al. 2008). In a follow-up to the present work, we plan to study the catalytic role of OCS in the peptide formation in ices of astrophysical interest.

In contrast, solid H_2S has never been identified in the interstellar medium (ISM), probably because its main band overlaps with a feature of CH_3OH (Garozzo et al. 2010; Jiménez-Escobar et al. 2011), one of the most abundant species detected in ice mantles (Dartois et al. 1999; Gibb et al. 2004; Mumma & Charnley 2011; Whittet et al. 2011). In this paper, we report the observation of efficient photodepletion yields for H_2S in CO:H_2S and CO_2:H_2S ice mixtures. The results could explain why this species has not been observed in ice mantles.

Until now, only proton irradiation of ices containing CO or CO_2 as the carbon source and H_2S or SO_2 as the sulfur

Table 1
Band Positions and Band Strengths (A) of the Starting Ice Components Used and the Photoproducts Identified in This Study

Molecules	Band position (cm^{-1})	A (cm molecule^{-1})	References
H_2S	2550	2.0×10^{-17}	Jiménez-Escobar & Muñoz Caro (2011)
CO_2	2345	7.6×10^{-17}	Yamada & Person (1964)
CO	2139	1.1×10^{-17}	Jiang et al. (1975)
^{13}CO	2092	1.1×10^{-17}	Jiang et al. (1975)
OCS	2050	1.5×10^{-16}	Hudgins et al. (1993)
CS_2	1520	9.13×10^{-17}	Pugh & Rao (1976)

source have been studied and reported for the formation of OCS (Ferrante et al. 2008; Garozzo et al. 2010). A UV-irradiation study of similar ice mixtures was, to our knowledge, not reported in the literature. In this work, we present a series of experiments using either a microwave-discharge hydrogen-flow lamp (MDHL), referred to as the VUV light source (simulating the interstellar UV field; Gredel et al. 1989; Cruz-Diaz et al. 2014a) or a monochromatic light (at wavelengths of 30.4 nm and 58.4 nm) provided by a synchrotron radiation, referred to as the EUV light source. According to observations, the prominent solar emission intensities at 30.4 nm (He II), 58.4 nm (He I), and 121.6 nm (Lyα) are 3.59×10^{13}, 9.57×10^{12}, and 3.25×10^{15} cm^{-2} s^{-1} sr^{-1}, respectively (Dupree & Reeves 1971). EUV photons can excite molecules to their ionization continua and dissociate them into neutral and ionic fragments, and that some molecular species may be synthesized after irradiation with EUV photons, but not necessarily after vacuum ultraviolet (VUV) irradiation (Wu et al. 2002).

2. EXPERIMENTAL

The experiments described in this work were performed using the Interstellar Photoprocess System (IPS). This setup and the experimental protocol are described in detail in Chen et al. (2014). Briefly, the IPS consists of an ultra-high-vacuum (UHV) chamber equipped with a closed-cycle helium cryostat, with a background pressure of $\sim 1 \times 10^{-10}$ torr. Ice films were deposited on a KBr window, which is attached to the tip of a cold finger. The temperature of the KBr window can be controlled by a tunable heater with a 0.1 K accuracy from 14 K to 400 K.

Gas mixtures were prepared in a gas handling system consisting of four stainless steel bottles of the same volume. The relative proportions between the mixture components were determined by their partial pressures. Gas mixtures were admitted and sprayed onto the KBr substrate in the UHV chamber via 1/4″ flexible stainless steel tube, and the flow rate was controlled with a leak valve. The chemical compounds used for these experiments were CO (Matheson, 99.99% purity), ^{13}CO (Specialty Gases of America, 99% purity), CO_2 (Matheson, 99.995% purity), and H_2S (Specialty Gases of America, 99.5% purity).

Ice mixtures in the UHV chamber were monitored by an in situ Fourier-transform infrared (FTIR) spectrometer equipped with a mercury–cadmium–telluride (MCT) detector and used in its transmission mode. Infrared spectra were acquired with a 4 cm^{-1} resolution and averaged over 128 scans. The photo- and thermo-desorbed species during photon irradiation and warm-up process were detected by quadrupole mass spectrometry (QMS). The column densities of each component of the deposited ice mixtures and of the photoproducts were calculated according to:

$$N = \int_{\text{band}} \frac{\tau_\nu \, d\nu}{A}, \quad \text{with } \tau_\nu = \ln (I_0/I), \tag{1}$$

where N is the column density in molecules cm^{-2}, τ_ν the optical depth of the band, ν the wavenumber in cm^{-1}, A the band strength in cm molecule^{-1}, and I_0 and I the intensities of the IR beam before and after passing through the ice sample, respectively. The band strengths used for the IR bands of H_2S, CO_2, CO, ^{13}CO, OCS, and CS_2 are listed in Table 1. Using the VUV absorption cross sections of CO and CO_2 reported by Cruz-Diaz et al. (2014a, 2014b), we estimated that the VUV photon absorption efficiency of CO ice in the 115−170 nm range is about 1 order of magnitude higher than that of CO_2 ice, so that in this study the column density of the deposited CO_2 was chosen to be about 10 times higher than that of CO.

The MDHL was used to provide VUV photons in the 114−180 nm range and its emission spectra in different operating configurations were discussed in detail in Chen et al. (2014). Typically, the MDHL provides hydrogen Lyα emission (H Lyα, 121.6 nm or 10.2 eV) and molecular H_2 emission in the 110–180 nm range (6.89−11.27 eV). In this study, two operating configurations of the MDHL equipped with MgF_2 and CaF_2 windows were chosen to provide VUV light sources with 8.4% of Lyα (with an average photon energy over the full emission range of 8.6 eV) and 0.0% of Lyα (same average photon energy), respectively, in order to determine the effect of Lyα photons on the photochemistry of CO:H_2S and CO_2:H_2S ice mixtures. The synchrotron radiation was produced by a 1.5 GeV electron storage ring at the National Synchrotron Radiation Research Center (NSRRC) in Hsinchu, Taiwan. The High Flux Cylindrical Grating Monochromator (HF-CGM) beamline provides photons with energies in the 5−45 eV range. A typical bandwidth (FWHM) of 0.4 nm in the EUV region was utilized in the present work. For this study, He I (21.2 eV, 58.4 nm) and He II (40.8 eV, 30.4 nm) were selected, with a photon flux of $\sim 1 \times 10^{14}$ photons cm^{-2} s^{-1}. In order to derive accurate photoproduction yields for products and photodepletion yields for parent molecules, an accurate measurement of the irradiation photon flux is required. Therefore, a calibrated nickel mesh, whose photoelectric efficiency is traceable to NIST standards, was installed in situ and was used to continuously record the photon flux during experimental runs.

3. RESULTS AND DISCUSSION

3.1. VUV Photon Irradiation of CO + H_2S and CO_2 + H_2S Ice Mixtures

3.1.1. Photolysis Products and Formation Mechanisms

Figure 1 shows the IR spectra of the CO:H_2S (20:1) and CO_2:H_2S (20:1) ice mixtures before and after VUV irradiation

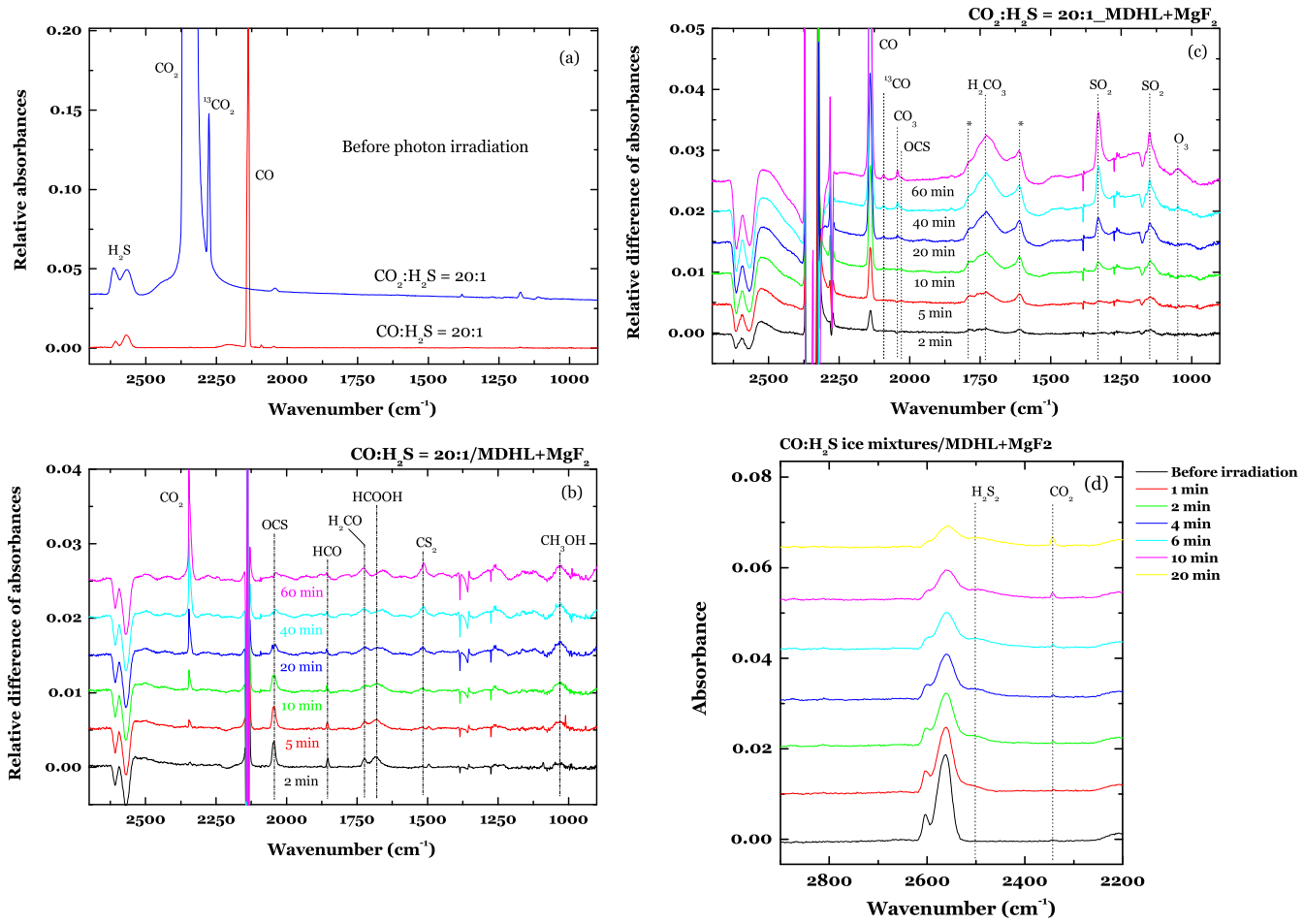

Figure 1. (a) IR spectra of the $CO:H_2S = 20:1$ and $CO_2:H_2S = 20:1$ ice mixtures before irradiation with the MDHL + MgF_2. (b) $CO:H_2S = 20:1$ ice mixture after irradiation. (c) $CO_2:H_2S = 20:1$ ice mixture after irradiation. (d) IR spectra of the $CO:H_2S$ ice mixtures plotted in absorbance, in order to emphasize the presence of the absorption band assigned to H_2S_2.

(MDHL + MgF_2) at 14 K. The measured spectral positions of products resulting from the VUV irradiation of $CO:H_2S$ (20:1) and $CO_2:H_2S$ (20:1) ice mixtures are listed in Tables 2 and 3, respectively. It must be mentioned that H_2S_2 is not easy to observe in the IR spectra plotted as the difference of absorbances, because its absorption peak overlaps that of H_2S, and thus its intensity is difficult to measure. Therefore, we calculated the absorption area of the H_2S_2 peaks from the IR spectra plotted in absorption, as the one shown in Figure 1(d). We note that CS_2 was only produced in the VUV-irradiated $CO:H_2S$ ice mixture, while SO_2 was only produced in the VUV-irradiated $CO_2:H_2S$ ice mixture. This result is in agreement with that of Ferrante et al. (2008), who used 0.8 MeV protons to irradiate $CO:H_2S$ (5:1) and $CO_2:H_2S$ (5:1) ice mixtures. However, it is quite different from the results of Garozzo et al. (2010), who used 0.2 MeV protons to irradiate a $CO:H_2S$ (10:1) ice mixture and reported the observation of SO_2, suggesting an effect of the ratio between the components in the starting mixtures.

The VUV light source employed in this study was MDHL equipped with an MgF_2 or a CaF_2 window has a cutoff wavelength at 114 nm (10.87 eV) and 123 nm (10.08 eV), respectively. Both photon energies are lower than the dissociation energy of CO at 11.09 eV (Okabe 1978). Therefore, O atoms cannot be produced in VUV-irradiated $CO:H_2S$ ice mixtures. However, the formation of SO_2 requires an oxygen-rich environment, as it is typically formed via the following reaction pathway (see Figure 2):

$$\begin{aligned} &CO_2 + h\nu \rightarrow CO + O \quad h\nu \geqslant 5.454 \text{ eV } (\leqslant 227 \text{ nm}) \\ &HS + O \rightarrow SO + H \\ &SO + O \rightarrow SO_2 \\ &SO + SO \rightarrow SO_2 + S. \end{aligned} \tag{2}$$

This may explain why SO_2 is produced in the MDHL irradiation of $CO_2:H_2S$ ice mixtures, but not when starting with an $CO:H_2S$ ice. In addition to Equation (2), there is another possible reaction

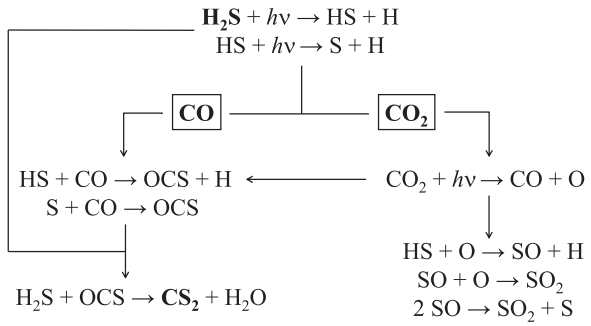

Figure 2. Reaction schemes of the species produced during VUV (MDHL + MgF_2 and MDHL + CaF_2) irradiation of the $CO:H_2S$ and $CO_2:H_2S$ ice mixtures.

Table 2
Products Identified in the IR Spectra of the CO: H_2S Ice Mixtures Irradiated with 30.4 nm (He II), 58.4 nm (He I), and the MDHL in the Configurations MDFL + MgF_2 and MDHL + CaF_2, and Comparison with Previous Studies

Ice mixture	Present work CO:H_2S				Ferrante et al. (2008) CO:H_2S	Garozzo et al. (2010) CO:H_2S
Mixture ratio	20:1	20:1	20:1	20:1	5:1	10:1
Energy source	30.4 nm	58.4 nm	MDHL + MgF_2	MDHL + CaF_2	0.8 MeV protons	0.2 MeV protons
Product	Peak position (cm^{-1})					
H_2S_2	2511	2511	2510	2508		2487
CO_2	2344	2344	2346	2345	2342	2345
$^{13}CO_2$						2280
C_3O_2	2242	2240			2242	2248
C_5O_2						2214
$OCC^{13}CO$	2192	2192				2192
C_7O_2						2122
C_5O_2						2070
OCS	2047	2045	2046	2045	2048	2043
C_2O	1988	1988			1990	1989
HCO	1855	1853	1853	1857	1859	1858
H_2CO	1716	1722	1724	1723	1712	
HCOOH	1679	1685	1686	1686		
CS_2	1521	1521	1515	1514	1524	1519
H_2CO	1495	1497	1496	1496	1496	
SO_2						1327
SO_2						1149
CH_3OH	1030	1030	1030	1030		
O_3						1044

Table 3
Products Identified in the IR Spectra of the CO_2:H_2S Ice Mixtures Irradiated with 30.4 nm (He II), 58.4 nm (He I), and the MDHL in the Configurations MDFL + MgF_2 and MDHL + CaF_2, and Comparison with Previous Study

Ice mixture	Present work CO_2:H_2S				Ferrante et al. (2008) CO_2:H_2S
Mixture ratio	20:1	20:1	20:1	20:1	5:1
Energy source	30.4 nm	58.4 nm	MDHL + MgF_2	MDHL + CaF_2	0.8 MeV Protons
Product	Peak position (cm^{-1})				
H_2S_2 (100 K)	2493	2495	2493	2493	
CO	2140	2140	2139	2141	2142
^{13}CO	2091	2094	2090	2092	
CO_3	2043	2044	2043	2044	2043
OCS	2040	2040	2042	2042	2048
H_2CO_3	1724	1729	1729	1730	
Uni.	1608	1613	1612	1608	
CS_2	1523	1519			
SO_2	1330	1330	1331	1332	1337
SO_2	1149	1150	1149	1148	1152
O_3	1045	1046	1049	1048	1044

pathway for its formation:

$$CO_2 + h\nu \rightarrow C + O_2 \quad h\nu \geqslant 11.43 \text{ eV } (\lambda \leqslant 108 \text{ nm})$$
$$S + O_2 \rightarrow SO_2. \quad (3)$$

The photon energy provided by the MDHL light source is clearly not sufficient to produce O_2 from the dissociation of CO_2. However, it is not an issue when EUV photons provided by the tunable synchrotron radiation source are used (see Section 3.2 for discussion).

Regarding the production of CS_2 in the photolysis of CO:H_2S ice mixtures, possible reaction pathways include:

$$H_2S + h\nu \rightarrow HS + H \quad h\nu \geqslant 3.26 \text{ eV } (\lambda \leqslant 317 \text{ nm})$$
$$HS + CO \rightarrow OCS + H$$
$$S + CO \rightarrow OCS$$
$$H_2S + OCS \rightarrow CS_2 + H_2O. \quad (4)$$

To test the above reaction pathways, we checked the production of H_2O. For this, two separate experiments were conducted on similarly prepared CO:H_2S ice samples, one subjected to VUV irradiation and another not irradiated (i.e., a blank experiment). The absorption band of H_2O spanning from 3000 to 3700 cm^{-1} and centered at 3370 cm^{-1} was selected for this study. The resulting column density of H_2O produced by VUV irradiation of CO:H_2S ice is plotted in Figure 3, along with that obtained from the blank experiment. In the latter case, the slight increase in the H_2O column density is attributed to condensation on the ice sample from residual H_2O (gas) inside the UHV chamber. However, from Figure 3, it clearly appears that the column density of H_2O in the CO:H_2S ice sample is much higher after VUV irradiation than that in the blank experiment. Thus, both CS_2 and H_2O are observed after the photolysis of CO:H_2S ice mixtures, which is consistent with the pathway described in

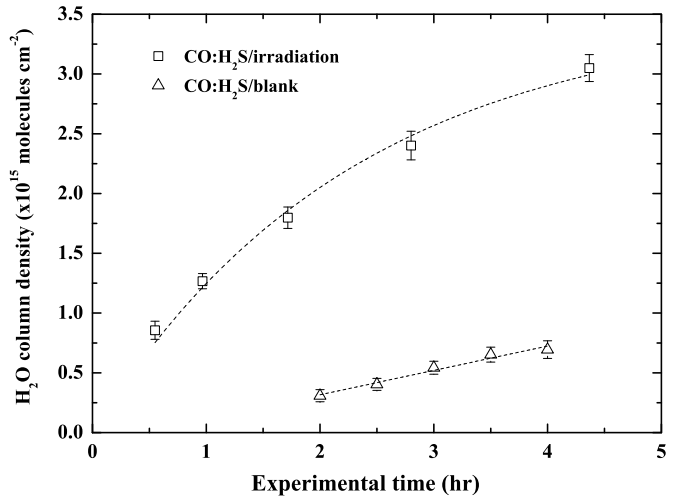

Figure 3. Column density of H_2O as a function of the experimental time for the experiments of the VUV irradiation (MDHL + MgF_2) of the CO:H_2S ice mixtures, and for the blank experiment (no irradiation) of the CO:H_2S ice mixture.

Equation (4). Another possible pathway for the production of CS_2 is:

$$\begin{aligned} &OCS + h\nu \rightarrow CS + O \quad h\nu \geqslant 5.33 \text{ eV } (\lambda \leqslant 182 \text{ nm}) \\ &CS + S \rightarrow CS_2. \end{aligned} \tag{5}$$

The CS radical is produced from the subsequent photodissociation of OCS, which competes with the reaction with H_2S (Equation (4)). Thus, this reaction will not contribute significantly to the production of CS_2, simply because the abundance of the starting H_2S molecules will be an order of magnitude higher than that of the produced OCS.

Ferrante et al. (2008) proposed that OCS_2 was produced by 0.8 MeV protons irradiation of pure OCS ice, and subsequent $OCS_2 \rightarrow O + CS_2$ dissociation would give CS_2. However, they did not observe OCS_2 formation in the 0.8 MeV protons irradiation of CO + H_2S ice mixtures experiment. Similarly, we could not identify any OCS_2 produced in our experiments of photo-irradiation of CO:H_2S ices.

The productions of OCS and CS_2, and the depletion of the starting compound H_2S upon photolysis of CO:H_2S ice mixtures (20:1 and 5:1), have been investigated in the present study. Figure 4 shows the normalized column densities of OCS and CS_2, i.e., their column densities divided by the initial column density of H_2S (before VUV irradiation), as a function of the photon dose. The depletion of H_2S at the beginning of the VUV irradiation (photon dose $<2.3 \times 10^{16}$ photons cm^{-2}) of both CO:H_2S ice mixtures is correlated with the production of OCS. When the photon dose reaches 2×10^{17} photons cm^{-2}, the column density of H_2S decreases to less than 10% of its initial value. In other words, more than 90% of the initial H_2S is depleted, while small quantities of OCS are produced. The initial production and depletion yields are summarized in Table 5.

The photo-induced depletion of the starting molecules can result from two independent processes, namely, photolysis and photo-induced desorption (also called photodesorption). Photolysis leads to the destruction of the starting molecules to convert them into products via radical–radical and radical–molecule reactions, whereas photodesorption does not involve any dissociation of the starting molecules but provides them with enough energy to be sputtered out of the ice surface and become free gas-phase particles (Chen et al. 2014). The production of CS_2 always begins after the column density of OCS reaches its maximum during the VUV irradiation experiments. This suggests that the formation of CS_2 is correlated with the destruction of OCS, as observed by Ferrante et al. (2008) in their proton irradiation experiments.

Table 4
Identified Products of the MDHL + MgF_2 Irradiation of the CO:H_2S and ^{13}CO:H_2S Ice Mixtures

Ice mixture	CO:H_2S = 20:1	^{13}CO:H_2S = 20:1
Product	Peak position (cm^{-1})	
H_2S_2	2510	2510
CO_2	2346	
$^{13}CO_2$		2280
OCS	2046	
$O^{13}CS$		1994
HCO	1853	
$H^{13}CO$		1814
H_2CO	1724	
$H_2{}^{13}CO$		1687
HCOOH	1686	
$H^{13}COOH$		1649
CS_2	1515	
$^{13}CS_2$		1464
CH_3OH	1030	
$^{13}CH_3OH$		1018

The products HCO, H_2CO, HCOOH, and CH_3OH were observed in the irradiated CO:H_2S ices, and were likely formed via the following reactions:

$$\begin{aligned} &H + CO \rightarrow HCO \\ &H + HCO \rightarrow H_2CO \\ &OH + HCO \rightarrow HCOOH \\ &H_2CO + 2\,H \rightarrow CH_3OH. \end{aligned} \tag{6}$$

In order to further confirm the identification of the products in the VUV-irradiated CO:H_2S ice mixtures, ^{12}CO was substituted by ^{13}CO in the sample preparation. Figure 5 shows that the carbon-containing products in the VUV-irradiated (MDHL + MgF_2) CO:H_2S ice, including OCS, HCO, H_2CO, and HCOOH, all display redshifted absorption features in the IR spectra of the VUV-irradiated ^{13}CO:H_2S ice experiment, as expected. Table 4 lists the absorption peak positions of all carbon containing products measured in the IR spectra of the VUV-irradiated CO:H_2S and ^{13}CO:H_2S ice experiments. It should be noted that Figure 5 does not show the absorption feature of CS_2, because the irradiation time was too short to reach the production column density of OCS required to form CS_2.

3.1.2. Effect of the Carbon Source on the Production of OCS

CO_3 can be produced in irradiated CO_2 ices (Jacox & Milligan 1971; Bennett et al. 2004). Its absorption feature at 2043 cm^{-1} is close to that of OCS at 2040 cm^{-1}, within the resolution of the present work. The asymmetric absorption band profile between 2080 and 2000 cm^{-1} could consist of absorption features of both CO_3 and OCS in the irradiated CO_2:H_2S (20:1) ice mixtures (Figure 6). To accurately measure the OCS absorbance and hence its column density, we separated the contributions from both absorption features. For this, the absorption band in the 2080–2000 cm^{-1} region was deconvoluted with two Gaussian functions. The sum of the two resulting fitted profiles (Figure 6,

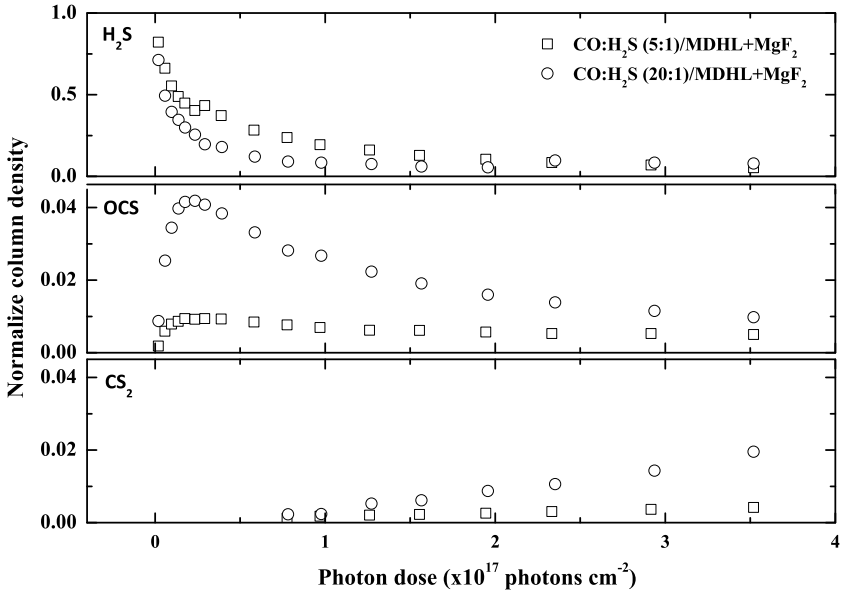

Figure 4. Normalized depletion column density of H_2S and normalized production column densities of OCS and CS_2 in the CO:H_2S = 5:1 (squares) and 20:1 (circles) ice mixtures irradiated with the MDHL + MgF_2 configuration as a function of the photon dose.

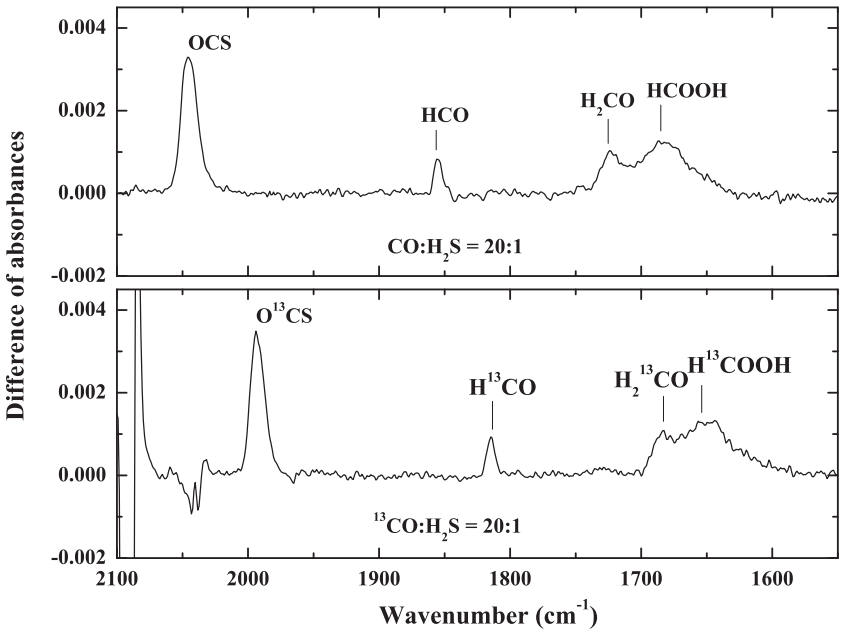

Figure 5. IR spectra of the MDHL + MgF_2 irradiated CO:H_2S (20:1) and ^{13}CO:H_2S (20:1) ice mixtures. The bands of ^{13}C-labeled photoproducts are, as expected, shifted to lower wavenumbers.

Table 5
Initial Production Yield of OCS and Depletion Yield of H_2S in the CO:H_2S (20:1) Ice Mixtures Irradiated with the VUV (MDHL + MgF_2 and MDHL + CaF_2) and EUV (30.4 nm and 58.4 nm) Light Sources

		Initial Production Yield of OCS (molecules photon^{-1})	Initial Depletion Yield of H_2S (molecules photon^{-1})
CO:H_2S = 20:1	MDHL + MgF_2	$(2.0 \pm 0.2) \times 10^{-2}$	$(1.5 \pm 0.2) \times 10^{-1}$
	MDHL + CaF_2	$(0.8 \pm 0.1) \times 10^{-2}$	$(0.5 \pm 0.1) \times 10^{-1}$
	30.4 nm	$(1.7 \pm 0.2) \times 10^{-2}$	$(1.6 \pm 0.3) \times 10^{-1}$
	58.4 nm	$(0.6 \pm 0.2) \times 10^{-2}$	$(0.4 \pm 0.1) \times 10^{-1}$

red curve) matches the IR band in the spectrum very well (black curve). The sharper peak, centered at 2043 cm^{-1} with a FWHM of 4 cm^{-1}, was assigned to CO_3, while the broader peak, centered at 2040 cm^{-1} with a FWHM of 20 cm^{-1}, was assigned to OCS. The fitted positions and bandwidths are in very good agreement with previously reported values (Hudgins et al. 1993; Ferrante et al. 2008). The uncertainty for the integrated absorbances was estimated to be better than 5% of the given fitted value.

The column densities of the OCS produced in the VUV-irradiated CO:H_2S (20:1) and CO_2:H_2S (20:1) ices were measured as a function of the photon dose. To present the production

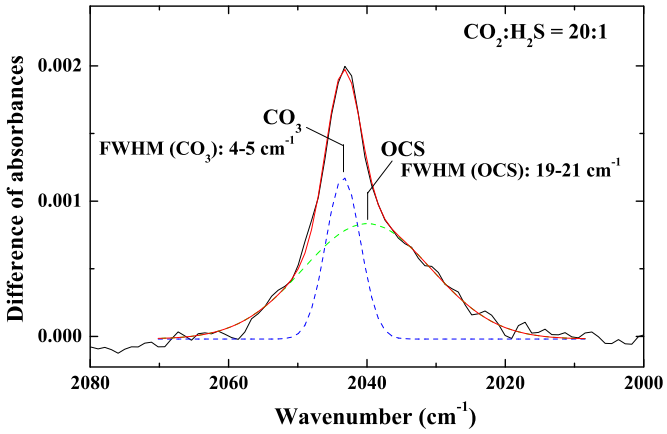

Figure 6. IR spectrum in the 2080–2000 cm^{-1} region of irradiated CO_2:H_2S ice showing how the bands of new photoproducts are fitted with Gaussian peaks to identify CO_3 and OCS.

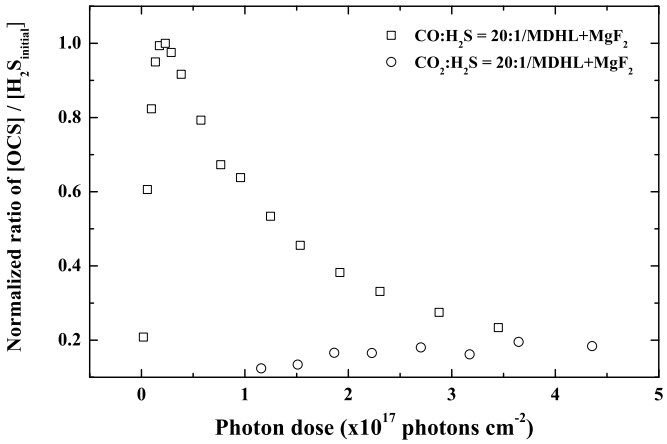

Figure 7. Evolution of the [OCS]/[$H_2S_{initial}$] ratio as a function of the photon dose during the VUV irradiation of CO:H_2S (20:1) and CO_2:H_2S (20:1) ice mixtures. Each data point is normalized to the maximum absorption band area of OCS in the CO:H_2S = 20:1 ice mixture.

efficiency of OCS in the VUV irradiation of CO:H_2S = 20:1 and CO_2:H_2S = 20:1 mixtures, a ratio of [OCS]/[$H_2S_{initial}$], namely, the OCS production column density divided by the initial column density of H_2S, is plotted in Figure 7. The production yield, namely, the number of molecules produced per incident photon, of OCS in CO:H_2S (20:1) ices is at least two orders of magnitude higher than that in CO_2:H_2S (20:1) ices. The maximum conversion of produced OCS from H_2S in the CO:H_2S (20:1) ices is about five times higher than that in the CO_2:H_2S (20:1) ices during VUV irradiation period. Ferrante et al. (2008) and Jiménez-Escobar et al. (2014) proposed the following reaction pathway for the formation of OCS:

$$\begin{aligned} &S + CO \rightarrow OCS \\ &HS + CO \rightarrow OCS + H. \end{aligned} \quad (7)$$

When CO_2:H_2S mixtures are used as starting compounds, CO must be formed first via photolysis of CO_2:

$$CO_2 + h\nu \rightarrow CO + O \quad h\nu \geqslant 5.454 \text{ eV } (\leqslant 227 \text{ nm}). \quad (8)$$

The O atoms produced will subsequently compete with CO to react with HS to form SO radicals. From Equations (7) and (8),

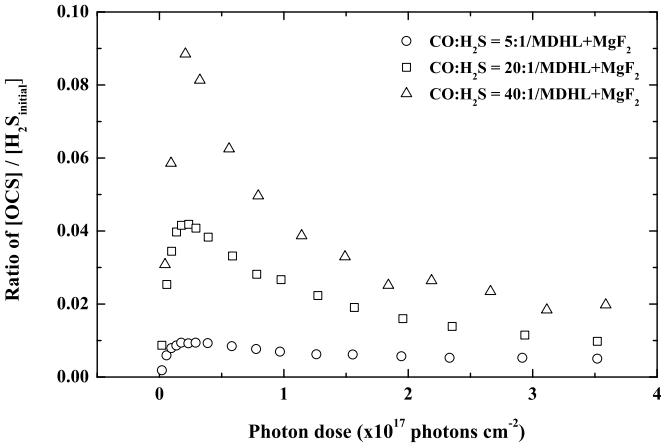

Figure 8. Evolution of the [OCS]/[$H_2S_{initial}$] ratio as a function of the photon dose during the VUV irradiation of the CO:H_2S ice mixtures with relative proportions 5:1 (squares), 20:1 (circles), and 40:1 (triangles).

it is easy to understand why the production yield of OCS in CO:H_2S ices is much higher than that in CO_2:H_2S ices.

3.1.3. Effect of the Concentration of H_2S on the Production of OCS

We have also performed VUV irradiation of CO:H_2S and CO_2:H_2S ice mixtures in several mixed proportions. To estimate the conversion percentage from H_2S into OCS, we have plotted the ratio of column densities [OCS]/[$H_2S_{initial}$] as a function of the photon dose in Figure 8. It shows that the maximum conversion percentage for the sulfur atoms in the starting H_2S into OCS are 4.2% and 1.0% in the VUV-irradiated (MDHL + MgF_2) CO:H_2S (20:1) and CO:H_2S (5:1) ice mixtures, respectively. A lower concentration of H_2S in a VUV-irradiated CO:H_2S ice led to a more efficient formation of OCS. This phenomenon was also observed in VUV-irradiated CO_2:H_2S ice mixtures with starting proportions up to 400:1.

To study how the sulfur concentration in the starting ice mixtures affects the production efficiencies of OCS and H_2S_2, we set a fixed initial ice column density of CO, so that different relative proportions between CO and H_2S in CO:H_2S ice mixtures will result in a change in the distance between two adjacent H_2S molecules in the ice matrix. Upon VUV photodissociation of H_2S, a shorter distance between two HS radicals would result in their easier recombination, while a longer distance between them would enhance reactions with CO in the ice matrix to form OCS. Since the IR absorption band strength of H_2S_2 is not available in the literature, we present the discussion in terms of the difference in the integrated absorbance, ΔA. Figure 9 shows the plots of ΔA (OCS at 2040 cm^{-1}) and ΔA(H_2S_2 at 2500 cm^{-1}) as a function of the photon dose, and indicates that the evolution of the H_2S_2 production relative to the CO concentration follows an opposite trend to that of OCS. This result supports our expectation that the formation of H_2S_2 competes efficiently with that of OCS, in particular for low CO concentrations. The values of ΔA(OCS) $\times$ ΔA(H_2S_2) for CO:H_2S = 5:1 and 20:1 ices are 0.0067 and 0.006, respectively, at a photon fluence of 2.4×10^{16} photons cm^{-2}. This is to say that the formation curves for OCS and H_2S_2 in CO:H_2S ices exhibit an anticorrelation relationship.

3.1.4. Effect of the Photon Energy on the Production of OCS

The products are similar in both the CO:H_2S and CO_2:H_2S ice mixtures when irradiated with the MDHL + MgF_2 (8.4% Ly;

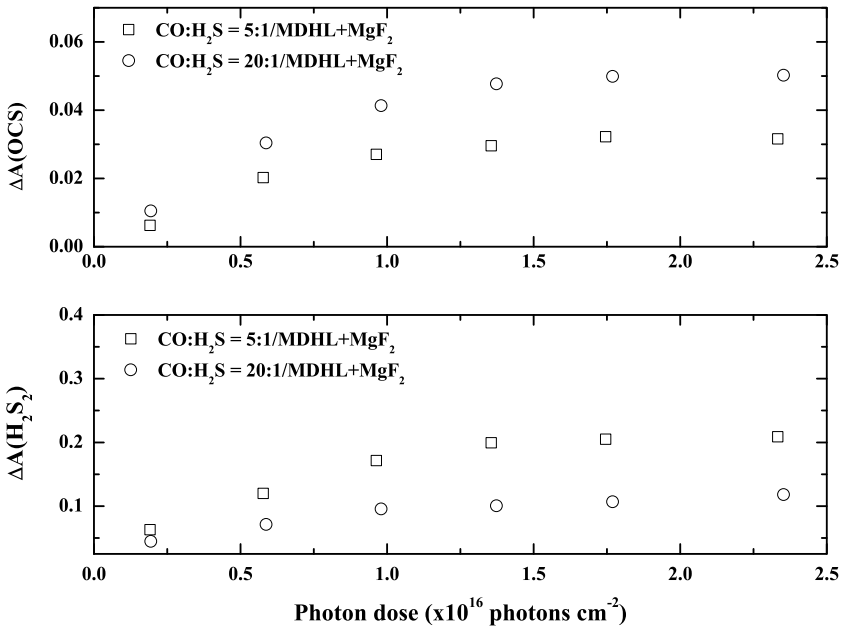

Figure 9. Trends of the difference of absorbances of OCS and H_2S_2 as a function of the photon dose for the VUV-irradiated CO:H_2S (5:1) and CO:H_2S (20:1) ice mixtures.

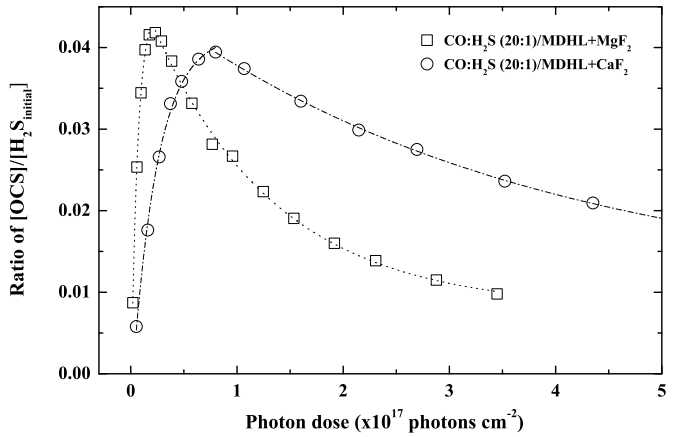

Figure 10. Evolution of the normalized column densities of OCS in the CO:H_2S ice mixtures irradiated with both configurations of VUV light sources (MDHL + MgF_2 and MDHL + CaF_2, which have different proportions of Lyα emission), as a function of the photon dose.

average photon energy: 8.6 eV) and MDHL + CaF_2 (0.0% Lyα; same average photon energy) light sources (see Tables 1 and 2). This result can be explained knowing that the dissociation energies of CO, CO_2, H_2S, and HS are 11.09 eV, 5.5 eV, 3.89 eV, and 3.63 eV, respectively (Okabe 1978; Peebles 2002). Indeed, CO cannot be dissociated upon MDHL irradiation in both operating configurations, but CO_2, H_2S, and HS are readily dissociated. Therefore, it is not surprising that similar products are formed when CO:H_2S and CO_2:H_2S ice mixtures are irradiated with VUV photons.

Figure 10 shows the [OCS]/[$H_2S_{initial}$] ratio in the CO:H_2S (20:1) ice mixture irradiated with the MDHL + MgF_2 and MDHL + CaF_2 light sources. The initial OCS production yields determined from Figure 10 are $(2.0 \pm 0.2) \times 10^{-2}$ and $(0.8 \pm 0.1) \times 10^{-2}$ molecules photon^{-1} for the MDHL + MgF_2 and MDHL + CaF_2 configurations, respectively. After OCS reaches its maximum abundance, the depletion yield of OCS upon MDHL + MgF_2 irradiation remains higher than that upon the MDHL + CaF_2 irradiation. Apparently, in this case the Lyα photons (8.4% vs. 0% in the two lamp configurations) play an important role in the ice photochemistry.

The absorption cross section of H_2S is almost constant in the 120–160 nm range (Cruz-Diaz et al. 2014a). This observation supports the similar H_2S photodepletion yields measured in both irradiation configurations. In our previous study, the conversion efficiency of CO ice to CO_2 was found to depend on photon energy, i.e., 5% by MDHL + MgF_2 and 12% by MDHL + CaF_2, respectively (Chen et al. 2014). The absorption cross section of CO ice at 121.6 nm (Lyα) is very small compared to those in the 140–160 nm region (molecular hydrogen emission bands; Lu et al. 2005; Cruz-Diaz et al. 2014a). Therefore, during VUV irradiation, CO molecules in CO:H_2S ice mixture contribute significantly to the production of OCS.

3.2. EUV Photon Irradiation of CO:H_2S and CO_2:H_2S Ice Mixtures

The effect of EUV irradiation on CO:H_2S and CO_2:H_2S ice mixtures was studied at NSRRC for two different photon wavelengths, 30.4 nm and 58.4 nm. Figure 11 shows the IR spectra of CO:H_2S (20:1) and CO_2:H_2S (20:1) ice mixtures at 14 K in the 2400–1000 cm^{-1} region obtained after EUV photon (30.4 nm, He II) irradiation. The photo-products identified in these irradiated ices are listed in Tables 1 and 2, respectively. There is a strong absorption feature around 1613 cm^{-1} which remains to be identified and was also observed in VUV-irradiated CO_2:H_2S (20:1) ices (see bottom panel of Figure 1c).

A closer look at the IR spectra shown in the top and bottom panels of Figures 11 reveals the striking ice photochemistry at work in the CO:H_2S (20:1) and CO_2:H_2S (20:1) ice mixtures. CS_2 was observed in both ice mixtures, while O_3 and SO_2 were only detected in the EUV-irradiated CO_2:H_2S ices. To better compare the data obtained between VUV and EUV irradiation, the [OCS]/[$H_2S_{initial}$] and [CS_2]/[$H_2S_{initial}$] ratios were plotted as a function of the photon dose in Figure 12. As discussed earlier, in the VUV-irradiation experiments, CS_2 was only produced in the CO:H_2S ice mixtures, and only after a significant

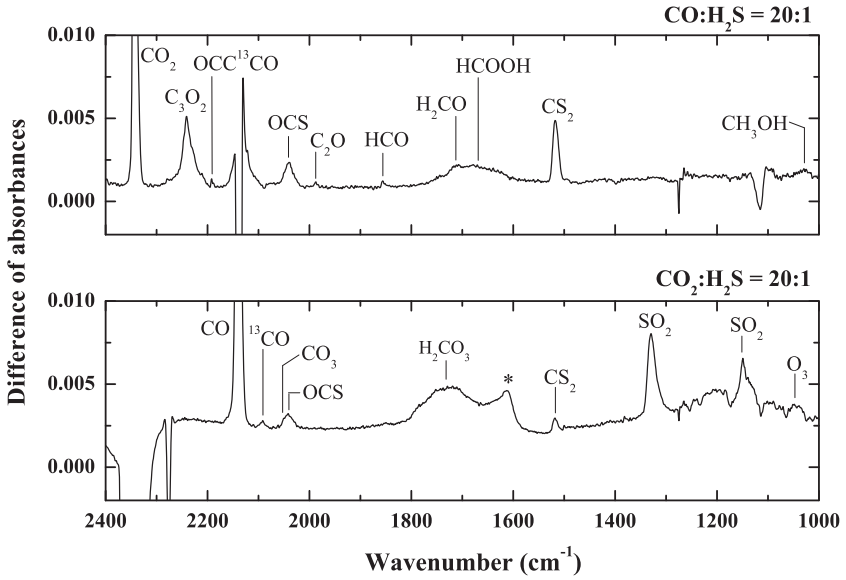

Figure 11. IR spectra of the CO:H_2S = 20:1 (top panel) and CO_2:H_2S = 20:1 ice mixtures (bottom panel) obtained after 30.4 nm photon irradiation.

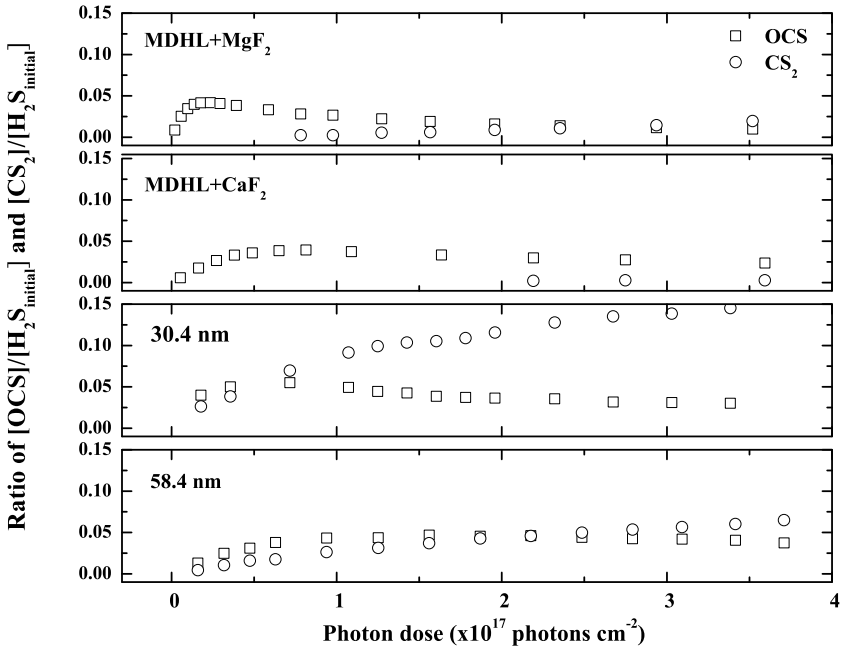

Figure 12. Evolution of the column densities of OCS and CS_2 in the CO:H_2S = 20:1 ice mixtures irradiated with the different light sources employed in the present study as a function of the photon dose.

amount of OCS was formed, which subsequently reacts with H_2S (see the top two panels of Figures 4 and 12). In contrast, in EUV-irradiation experiments, CS_2 is readily produced at the beginning of the irradiation of the CO:H_2S ice mixtures as well as in the CO_2:H_2S ice mixtures. Furthermore, Figure 12 shows that in the cases of 30.4 nm and 58.4 nm irradiations of CO:H_2S (20:1) ice, the production column density of CS_2 increases even when the column density of the produced OCS starts to decrease. The maximum production yield of CS_2 is about three times higher than that of OCS in the 30.4 nm irradiation experiment, which suggests that OCS is not necessarily required for the formation of CS_2 in the EUV irradiation experiments. Since the dissociation energy of CO is 11.09 eV, as mentioned earlier, it can be dissociated to form C and O upon EUV irradiation in both CO and CO_2 containing ice mixtures. The formation of CS_2 in EUV-irradiated CO:H_2S and CO_2:H_2S ice mixtures can occur via Equations (4) and (5), as well as the following additional reaction pathway:

$$\begin{aligned} &HS + O \rightarrow SO + H \\ &SO + C + CS + O \\ &CS + S \rightarrow CS_2. \end{aligned} \quad (9)$$

The HS radicals and S atoms produced from EUV photodissociated H_2S have been highlighted in Figures 2 and 13.

The influence of the carbon source and of the H_2S concentration on the production of OCS is comparable in EUV and VUV irradiation experiments. The production yield of OCS from the EUV irradiation of CO:H_2S ices is higher than for CO_2:H_2S ices. The initial production yields of OCS for 30.4 nm and 58.4 nm irradiations of CO:H_2S (20:1) ices were calculated

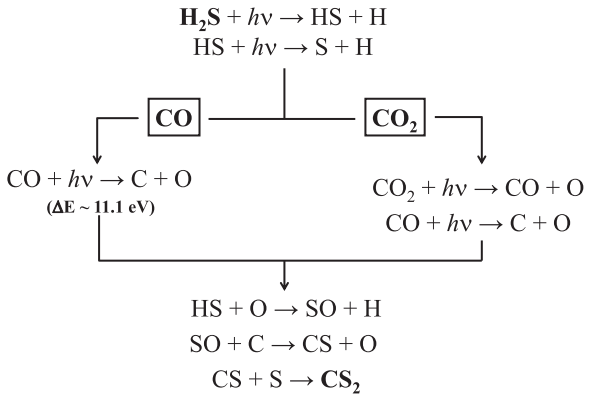

Figure 13. Reaction schemes of the species produced during EUV irradiation (30.4 nm and 58.4 nm) of the CO:H_2S and CO_2:H_2S ice mixtures.

to be $(1.7 \pm 0.2) \times 10^{-2}$ and $(0.6 \pm 0.1) \times 10^{-2}$ molecules photon^{-1}, respectively, indicating that a low concentration of H_2S in the CO:H_2S ice mixtures leads to a more efficient OCS formation.

3.3. The Missing Sulfur Atoms

In this section, we will determine the total conversion of H_2S in CO:H_2S (20:1) ice mixtures into S-containing products. As summarized in Table 1, the S-containing products we are interested in include H_2S_2, OCS, and CS_2. The conversion efficiency can be defined as the sum of the production column densities for H_2S_2, OCS, and CS_2 divided by the initial column density of H_2S, i.e., $H_2S_{initial}$. In this estimate, the contribution from H_2S_2 was not included because its infrared band strength is not known, so that the conversion data derived here represents only a lower limit. The results are plotted in Figure 14, and show that this conversion efficiency is lower than 5% for the VUV irradiation (MDHL + MgF_2) of a CO:H_2S (20:1) ice mixture (Figure 14(a)), while it is lower than 17% in the case of the 30.4 nm irradiation (Figure 14(b)). The conversion efficiency of S atoms from H_2S in the ice mixtures into S-containing photo-products is higher when 30.4 nm photons are used than in the case of an irradiation with the MDHL. These results are consistent with the fact that higher amounts of CS_2 are produced upon EUV irradiation (compare Figures 12 and 14(b)).

This raises a question about the missing S atoms in the photolysis of CO:H_2S and CO_2:H_2S ices. Barnes et al. (1974) reported that S- or HS-containing species such as H_2S_2 and S_2 are responsible for the formation of S-polymers up to S_8. Palumbo et al. (1997) suggested that S_8 might be formed by UV or cosmic-ray processing of sulfur-bearing molecules in icy grain mantles. However, since S_8 is a monovalent crystal, it has no IR active modes. Therefore, it cannot be detected directly via astronomical observations. Muñoz Caro (2002) reported that the UV irradiation of H_2S ice leads to the formation of S-polymers, which were detected in the resulting residues at room temperature by chromatographic techniques. Jiménez-Escobar & Muñoz Caro (2011) detected S_2 and S_3 in UV-irradiated H_2S and H_2O:H_2S ices during warm-up of their photolyzed ices by utilizing a mass spectrometer.

In order to verify whether other sulfur-bearing molecules are also present in our photolyzed ices, we have performed experiments using the VUV light source (MDHL + MgF_2) to irradiate a pure H_2S ice and a CO:H_2S (20:1) ice mixture. After a total photon dose of 2×10^{18} photons cm^{-2}, the ices were allowed to slowly warm up at a rate of 2 K min^{-1}

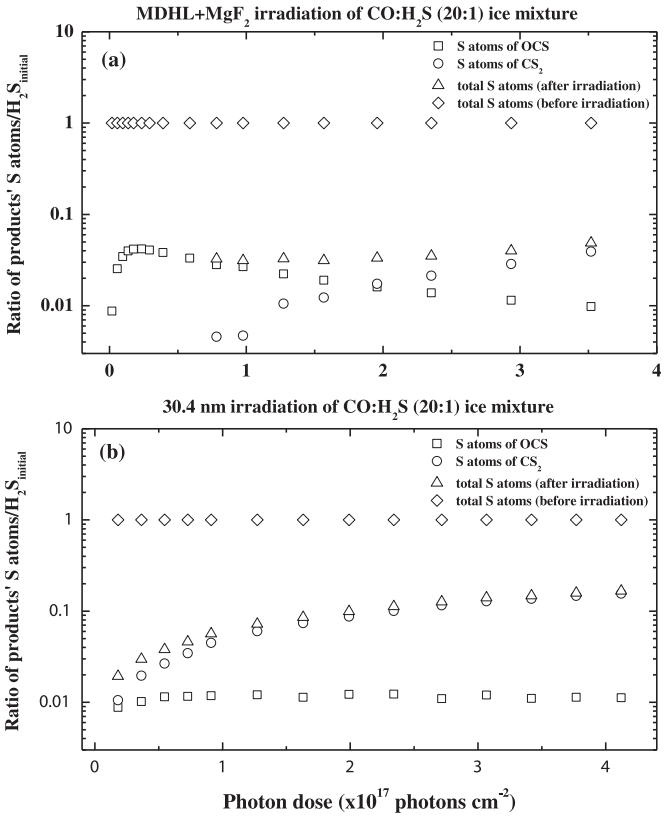

Figure 14. Ratio of the total and partial production column densities of S atoms in sulfur-containing products to the initial column density of H_2S in the CO:H_2S = 20:1 ice mixtures as a function of the photon dose: (a) MDHL + MgF_2 and (b) 30.4 nm irradiation.

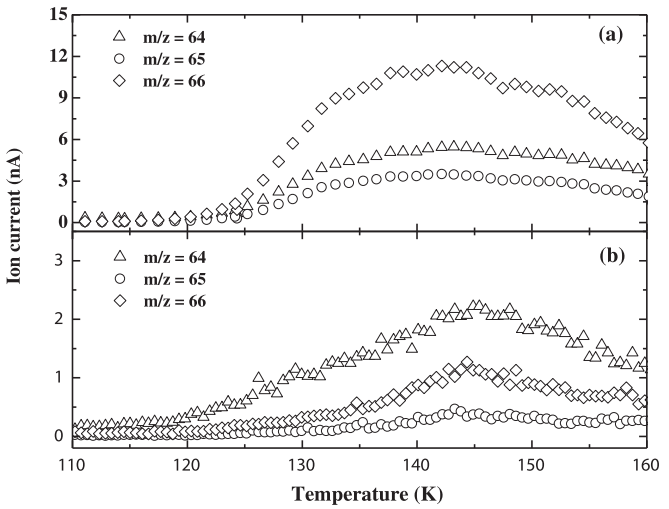

Figure 15. Evolution of the ion currents for $m/z = 64$, 65, and 66 (corresponding to S_2, HS_2, and H_2S_2, respectively) during the warm-up of the photolyzed ices of (a) pure H_2S ice and (b) CO:H_2S (20:1) ice mixtures after irradiation with the MDHL + MgF_2 light source.

and the desorbed gases were monitored by a quadrupole mass spectrometer (QMS). The ion currents measured by the QMS for $m/z = 64$, 65, and 66 (corresponding to S_2, HS_2, and H_2S_2) as a function of the lapse of warm-up time are shown in Figure 15. In the case of the photolyzed ices of pure H_2S ice the signals for ion currents at $m/z = 64$, 65, and 66 are in relative proportions of 0.48:0.31:1, indicating that H_2S_2 ($m/z = 66$) is the most abundant species. The signals of these ion currents reach a

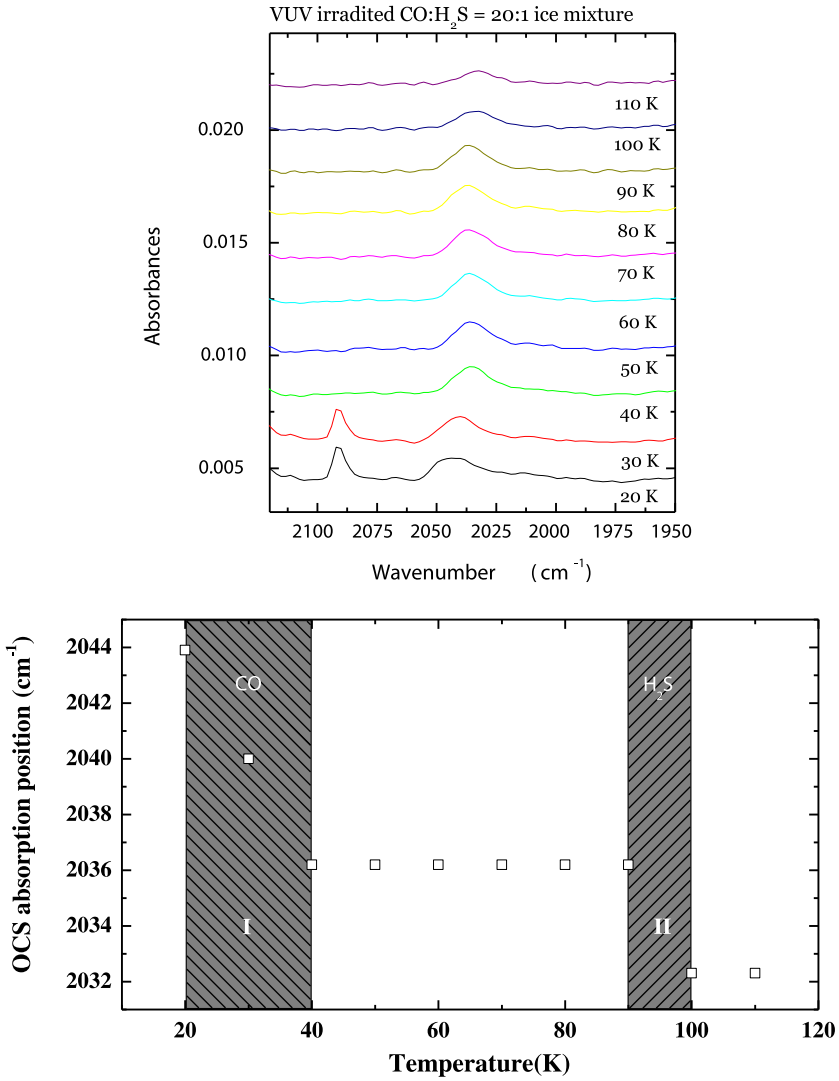

Figure 16. Measured infrared band positions of OCS in CO:H_2S = 20:1 ices after photolysis as a function of the temperature during ice warm-up. Regions I and II (shaded areas in the bottom panel) refer to the sublimation temperature ranges for CO and H_2S, respectively.

maximum around a temperature of 135−145 K. In the case of the irradiated CO:H_2S (20:1) ice mixture, the ion currents at m/z = 64, 65, and 66 during warm-up are plotted in Figure 15(b). As can be seen, the ion current for $m/z = 64$ is the highest. This result implies that there is at least one more species in the ice samples contributing to the signal of $m/z = 64$ (namely, S_2). The maximum signal of the ion currents centers around 140–150 K, which appears to agree with the observation of S_2 fluorescence during warm up by Grim et al. (1987), who reported a thermo-desorption temperature for S_2 around 150 K. Therefore, in the present work a fraction of the missing S atoms might be released in the form of S_2 from the photolyzed S-bearing products.

3.4. Effect of the Temperature on the OCS Spectra

In this study, the infrared band position of OCS was measured in CO:H_2S and CO_2:H_2S ice mixtures after irradiation when a total photon dose of 1×10^{18} photons cm^{-2} was reached. The results show that in CO:H_2S ices, these band positions depend on the temperature of the ice and the relative proportions between CO and H_2S in the starting mixture. The OCS band at 2044 cm^{-1} is redshifted as the temperature increases from 20 K to 110 K (Figure 16). In the 20–40 K temperature region during which CO starts to sublimate, the position of the OCS band shifts from 2044 cm^{-1} to 2036 cm^{-1} in the CO:H_2S (20:1) ice. In the 90–100 K region, during which H_2S sublimates, the position of the OCS band shifts from 2036 cm^{-1} to 2032 cm^{-1}. In contrast, the position of the OCS band at 2042 cm^{-1} does not change in the same temperature range in the CO_2:H_2S ice mixtures, regardless of the relative proportions between CO_2 and H_2S, which range from 400:1 to 5:1. Such a temperature-dependent data set may help unveil the thermal history of ice mixtures containing OCS molecules.

4. CONCLUSIONS AND RELEVANCE TO ASTRONOMICAL OBSERVATIONS

In this work, we studied the effects of the hydrogen sulfide concentration and the photon energy on the production of photoproducts from the irradiation of CO:H_2S and CO_2:H_2S ice mixtures. Our experimental results show that the depletion of the starting H_2S in CO:H_2S (20:1) and CO_2:H_2S (20:1) ices is rapid and reaches 90% even after irradiation with relatively low photon doses ($\sim2\times10^{17}$ photons cm^{-2}), which may explain why H_2S has not been observed in the solid phase in the ISM. The production yield of the photoproduct OCS reaches

maxima of about 5% and 1% relative to the initial S-atom content in CO:H_2S (20:1) and CO:H_2S (5:1) ices, respectively. This yield depends on the carbon source, as it is formed more efficiently in CO:H_2S ices than in CO_2:H_2S ices, as well as on the concentration of starting H_2S, as it increases when the concentration of H_2S decreases. One likely explanation for this is that the formation of OCS competes with that of H_2S_2. However, the total production of OCS seems to be independent of the photon energy range (VUV or EUV) of the incident light source, regardless of the relative proportions between the ice components in CO:H_2S and CO_2:H_2S mixtures.

OCS_2, a possible precursor of CS_2, was not observed in any of the CO:H_2S and CO_2:H_2S ice mixtures irradiated with VUV or EUV photons. In contrast, CS_2 where observed, probably formed from the reaction of OCS with H_2S, though its formation mechanism in EUV-irradiation experiments differs from that in the VUV-irradiation experiments. The main difference comes from the fact that CO, a precursor of CS_2, can only be dissociated by EUV photons because the energy of VUV photons is too low. The production yield of CS_2 was found to be higher than that of OCS in the EUV irradiation experiments, which is in agreement with previous experiments of irradiation of CO:H_2S (10:1) ices with 0.2 MeV protons.

The total quantities of detected S-containing products only amount for 5% and 17% of the S atoms in the starting CO:H_2S ices irradiated by VUV and EUV photons, respectively. S_2 was detected at a temperature of ~150 K during the warm-up of the photo-irradiated CO:H_2S ices, but no heavier S-polymers were observed, probably because of their low volatilities.

UV and X-ray irradiation of H_2S in the ice mixtures are known to lead to the production of H_2S_2, which can subsequently be photodissociated into S_2, and could explain the detection of S_2 in comets (Jiménez-Escobar & Muñoz Caro 2011; Jiménez-Escobar et al. 2012). In addition, CS_2 was also proposed as a parent molecule for S_2 in comets (A'Hearn et al. 1983), so that S_2, together with heavier S-polymers, may be formed on the surface of cold, ice-covered grains via VUV, EUV, and/or X-ray irradiation of mixtures containing H_2S and CO/CO_2.

Comparison between the IR spectra of ices observed toward the protostellar sources AFGL 989, Mon R2 IRS 2, and W33A with laboratory data of ices shows that the best fit to the astronomical observations is obtained if ices include OCS in the H_2O:CH_3OH mixtures (Palumbo et al. 1997). Experiments of irradiation of H_2O:CO:H_2S ices with 0.8 MeV protons indicated that the position of the IR band of the produced OCS was a very good match to that observed in the spectra of W33A at 4.90 μm (Ferrante et al. 2008). In the present work, the band position was found to vary significantly with the temperature during the warm-up after irradiation of the ices, ranging from 2044 cm^{-1} at 20 K to 2040 cm^{-1} at 30 K, which is in good agreement with the 2041 cm^{-1} feature for OCS observed toward W33A (Palumbo et al. 1997). Finally, our laboratory results support the abundance ratio N(CO)/N(OCS) of 20 in W33A estimated by Palumbo et al. (1997).

This work was supported by the NSC grant No. 101-2811-M-008-023 (T.-S.Y.), and NCU under the grant of The Aim for the Top University Project (W.-H.I.), the Spanish MICINN/MINECO under projects AYA2011-29375 and CSD2009-00038 (G.M.M.C.), and the NSF Planetary Astronomy Program under Grant AST-1108898 (C.-Y.R.W.). We acknowledge NSRRC for provision of synchrotron radiation facilities, as well as Dr. Bing-Ming Cheng for technical help on the beamline HF-CGM.

REFERENCES

A'Hearn, M. F., Schleicher, D. G., & Feldman, P. D. 1983, ApJL, 274, L99
Barnes, A. J., Hallam, H. E., & Howels, J. D. R. 1974, JMoSt, 23, 463
Bennett, C. J., Jamieson, C., Mebel, A. M., & Kaiser, R. I. 2004, PCCP, 6, 735
Bernstein, M. P., Dworkin, J. P., Sandford, S. A., et al. 2002, Natur, 416, 401
Boogert, A. C. A., Schutte, W. A., Helmich, F. P., Tielens, A. G. G. M., & Wooden, D. H. 1997, A&A, 317, 929
Boogert, A. C. A., Schutte, W. A., Tielens, A. G. G. M., et al. 1996, A&A, 315, L377
Chen, Y.-J., Chuang, K.-J., Muñoz Caro, G. M., et al. 2014, ApJ, 781, 15
Chen, Y.-J., Nuevo, M., Yih, T.-S., et al. 2008, MNRAS, 384, 605
Cruz-Diaz, G. A., Muñoz Caro, G. M., Chen, Y.-J., & Yih, T.-S. 2014a, A&A, 562, A119
Cruz-Diaz, G. A., Muñoz Caro, G. M., Chen, Y.-J., & Yih, T.-S. 2014b, A&A, 562, A120
Dartois, E., Schutte, W., Geballe, T. R., et al. 1999, A&A, 342, L32
Doty, S. D., Schoier, F. L., & van Dishoeck, E. F. 2004, A&A, 418, 1021
Dupree, A. K., & Reeves, E. M. 1971, ApJ, 165, 599
Ferrante, R. F., Moore, M. H., Spiliotis, M. M., & Hudson, R. L. 2008, ApJ, 684, 1210
Garozzo, M., Fulvio, D., Kanuchova, Z., et al. 2010, A&A, 509, A67
Gibb, E. L., Whittet, D. C. B., Boogert, A. C. A., & Tielens, A. G. G. M. 2004, ApJS, 151, 35
Gredel, R., Lepp, S., & Dalgarno, A. 1989, ApJ, 347, 289
Grim, R. J. A., & Greenberg, J. M. 1987, A&A, 181, 155
Hudgins, D. M., Sandford, S. A., Allamandola, L. J., & Tielens, A. G. G. M. 1993, ApJS, 86, 713
Jacox, M. E., & Milligan, D. E. 1971, JChPh, 54, 919
Jiang, G. J., Person, W. B., & Brown, K. G. 1975, JChPh, 62, 1201
Jiménez-Escobar, A., & Muñoz Caro, G. M. 2011, A&A, 536, A91
Jiménez-Escobar, A., Muñoz Caro, G. M., Ciaravella, A., et al. 2012, ApJL, 751, L40
Jiménez-Escobar, A., Muñoz Caro, G. M., & Chen, Y.-J. 2014, MNRAS, 443, 343
Leman, L., Orgel, L., & Ghadiri, M. R. 2004, Sci, 306, 283
Lu, H.-C., Chen, H.-K., Cheng, B.-M., et al. 2005, JPhB, 38, 3693
Millar, T. J., & Herbst, E. 1990, A&A, 231, 466
Mumma, M. J., & Charnley, S. B. 2011, ARA&A, 49, 471
Muñoz Caro, G. M. 2002, PhD thesis, Leiden Univ.
Muñoz Caro, G. M., Meierhenrich, U. J., Schutte, W. A., et al. 2002, Natur, 416, 403
Nuevo, M., Auger, G., Blanot, D., & d'Hendecourt, L. 2008, OLEB, 38, 37
Nuevo, M., Chen, Y.-J., Yih, T.-S., et al. 2007, AdSpR, 40, 1628
Palumbo, M. E., Tielens, A. G. G. M., & Tokunaga, A. T. 1995, ApJ, 449, 674
Okabe, H. 1978, Photochemistry of Small Molecules (New York: John Wiley & Sons)
Palumbo, M. E., Geballe, T. R., & Tielens, A. G. G. M. 1997, ApJ, 479, 839
Palumbo, M. E., Tielens, A. G. G. M., & Tokunaga, A. T. 1995, ApJ, 449, 674
Peebles, L. R., & Marshall, P. 2002, JChPh, 117, 3132
Pugh, L. A., & Rao, K. N. 1976, Molecular Spectroscopy: Modern Research, II (New York: Academic)
van der Tak, F. F. S., Boonman, A. M. S., Braakman, R., & van Dishoeck, E. F. 2003, A&A, 412, 133
Whittet, D. C. B., Cook, A. M., Herbst, E., et al. 2011, ApJ, 742, 28
Wu, C.-Y. R., Judge, D. L., Cheng, B.-M., et al. 2002, Icar, 156, 456
Yamada, H., & Person, W. B. 1964, JChPh, 41, 2478
Zasowski, G., Kemper, F., Watson, D. M., et al. 2009, ApJ, 694, 459